Output Tracking: Control of a VTOL

Shuyu Xia, David Tzer Chyi Yee, Qiubao Ye
Mechanical Engineering Department

I. System Description

The system chosen for this project was a Vertical Takeoff and Landing (VTOL) aircraft. Examples of such aircraft include the Boeing AV-8B Harrier depicted in Figure 1, Unmanned Aerial Vehicles (UAV), drones, or any other aircraft capable of taking off and landing vertically. Specifically, the VTOL aircraft investigated was the Harrier Jet which is a subsonic, single seat fighter utilizing a single turbofan engine for gross thrust generation. The Harrier's ability to take off vertically offers strategic advantages because it is requires very little area to operate. The United States Navy and Marine Corps operate the Harrier fighters from aircraft carriers which adds another benefit in fuel savings since a fleet of the aircraft can be transported on a single aircraft carrier and deployed from almost anywhere in the world.

Thrust from the single Rolls-Royce Phantom turbofan engine can be directed by modulating four synchronized exhaust nozzles which, depending on their positions, provide necessary thrust for full wing-borne flight, full jet-borne flight, or a combination of the two. By simultaneously rotating the positions of the two forward nozzles to point primarily in the vertical direction, the Harrier is capable of taking off, landing, and hovering in a vertical fashion. Reaction Control nozzles routing compressor bleed air from the engine are positioned at the wing tips, nose, and tail to provide reaction moments in the yaw, pitch, and roll directions during jet-borne and transitional flight making the aircraft fully controllable in the three rotational axes[1].

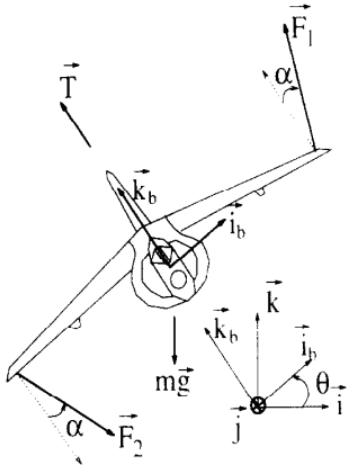

Figure .1. Diagram of a Vertical Take-off and Landing Aircraft

The variability of the throttle position, nozzle position, and roll, pitch, and yaw controls allow any moment and force to be generated on the aircraft's center of mass, up to physical saturation limits of the inputs. Of main importance in the model of the VTOL aircraft is the existence of a rolling moment-lateral force coupling. This cross coupling causes the system model to exhibit non-minimum phase behaviors which exclude conventional feedback control systems from being employed to control the planar motion of the aircraft.

II. System Model

In order to simplify the model for educational purposes, key assumptions and simplifications were made. The modeled aircraft is assumed to be a rigid body. Therefore, any deflections in the structure are assumed to be zero. In addition, internal dynamics of subsystems such as control surface actuators, the engine, etc. are neglected for the purpose of this project. This allows the control system to be applied to the high-level aircraft model, and the important overall dynamics of the aircraft can be realized.

The aircraft dynamics are modeled using two coordinate frames. Let the unit direction vectors (**i, j, k**) represent the bases for the fixed inertial coordinate frame and ($\mathbf{i}_b$, $\mathbf{j}_b$, $\mathbf{k}_b$) represent the bases for the moving coordinate frame attached to the aircraft's center of gravity (body axis). Based on the free body diagram in Figure 1, the forces acting on the system are

$$\boldsymbol{T} = T\,\boldsymbol{k}_b$$
$$\boldsymbol{F_1} = (\sin(\alpha)\,\boldsymbol{i}_b + \cos(\alpha)\,\boldsymbol{k}_b)F$$
$$\boldsymbol{F_2} = (\sin(\alpha)\,\boldsymbol{i}_b - \cos(\alpha)\,\boldsymbol{k}_b)F$$
$$m\boldsymbol{g} = mg\boldsymbol{k}$$

The equations of motion acting upon the center of mass are given by [2]

$$m(\ddot{x}\boldsymbol{i} + \ddot{y}\boldsymbol{k}) = T\boldsymbol{k}_b + 2\boldsymbol{F}\sin(\alpha)\,\boldsymbol{i}_b - mg\boldsymbol{k}$$
$$-J\ddot{\theta}\boldsymbol{j}_b = -2lcos(\alpha)\boldsymbol{F}\,\boldsymbol{j}_b$$

$J = moment\ of\ inertia\ about\ aircraft\ center\ of\ mass$
$m = mass\ of\ aircraft$
$\alpha = angle\ of\ tip\ force\ relative\ to\ body\ coordinate\ vertical\ direction$
$T = vertical\ thrust\ force$
$l = distance\ from\ center\ of\ mass\ to\ where\ forces\ F\ are\ applied$

Converting the applied forces to the fixed coordinate reference frame results in the following equations for the system dynamics:

$$\ddot{x} = -u_1 \sin(\theta) + \varepsilon u_2 \cos(\theta)$$
$$\ddot{z} = u_1 \cos(\theta) + \varepsilon u_2 \sin(\theta) - g$$
$$\ddot{\theta} = \lambda u_2$$

Where

$$u_1 = \frac{T}{m}$$

$$u_2 = \frac{2F}{m}\cos(\alpha)$$

$$\varepsilon = \tan(\alpha)$$

$$\lambda = \frac{ml}{J}$$

The system is thus modeled as a non-linear Multi Input-Multi Output (MIMO) system with state equations given by

$$\frac{d}{dt}\begin{bmatrix} x \\ \dot{x} \\ z \\ \dot{z} \\ \theta \\ \dot{\theta} \end{bmatrix} = \begin{bmatrix} \dot{x} \\ 0 \\ \dot{z} \\ -g \\ \dot{\theta} \\ 0 \end{bmatrix} + \begin{bmatrix} 0 & 0 \\ -\frac{\sin(\theta)}{m} & \frac{\varepsilon\cos(\theta)}{m} \\ 0 & 0 \\ \frac{\cos(\theta)}{m} & \frac{\varepsilon\sin(\theta)}{m} \\ 0 & 0 \\ 0 & \frac{\lambda}{J} \end{bmatrix} \begin{bmatrix} U_1 \\ U_2 \end{bmatrix}$$

The two inputs are the main thrust force U_1 and the rolling moment U_2 generated by the two forward exhaust nozzles located on both sides of the fuselage. The two outputs are the lateral position x and the vertical position z, or

$$y = \begin{bmatrix} 1 & 0 & 0 & 0 & 0 & 0 \\ 0 & 0 & 1 & 0 & 0 & 0 \end{bmatrix} \begin{bmatrix} x \\ \dot{x} \\ z \\ \dot{z} \\ \theta \\ \dot{\theta} \end{bmatrix}$$

The full state is hence

$$X = \begin{bmatrix} x \\ \dot{x} \\ z \\ \dot{z} \\ \theta \\ \dot{\theta} \end{bmatrix}$$

x = Lateral Position
$\dot{x}$ = Lateral Velocity
z = Vertical Position
$\dot{z}$ = Vertical Velocity
θ = Roll Angle
$\dot{\theta}$ = Roll Velocity

In the simulations, the parameters were selected to be as follows:

m = 1
J = 1
λ = 1
g = 9.81
ε = Varied

The coupling term ε was chosen a parameter to be varied in order to study its effects on the system tracking performance. Higher values of the force-moment coupling term resulted in increased non-minimum phase behaviors of the system because of the increased non-linearity it produced in the system's dynamics. In physical aircraft, the coupling term is small, usually on the order of 0.05 to 0.1. For the simulations, values of epsilon ranged up to 0.5.

III. Inversion Description

3.1 Iterative Approach

Based on the PVTOL state space, the relationship between the input and output can be found by differentiating the output twice and substituting for expressions from the state equation. Then, we have the inverse input as:

$$U_{ff} = \begin{bmatrix} U_1 \\ U_2 \end{bmatrix} = \begin{bmatrix} -\sin\theta & \varepsilon\cos\theta \\ \cos\theta & \varepsilon\sin\theta \end{bmatrix}^{-1} \begin{bmatrix} M\ddot{x}_d \\ M\ddot{z}_d + Mg \end{bmatrix}$$

$$= \frac{1}{\varepsilon} \begin{bmatrix} -\varepsilon\sin\theta & \varepsilon\cos\theta \\ \cos\theta & \sin\theta \end{bmatrix} \begin{bmatrix} M\ddot{x}_d \\ M\ddot{z}_d + Mg \end{bmatrix}$$

And the dynamics of the internal state can be found by substituting the inverse input into the expression in the equation as:

$$\frac{d}{dt}\eta = \begin{bmatrix} \eta_2 \\ \dfrac{\lambda M\ddot{x}_d \cos\eta_1}{J\varepsilon} + \dfrac{\lambda\left(M\ddot{z}_d + Mg\right)\sin\eta_1}{J\varepsilon} \end{bmatrix} = s\left[\eta, y_d\right]$$

Where

$$\eta = \begin{bmatrix} \eta_1 \\ \eta_2 \end{bmatrix} = \begin{bmatrix} \theta \\ \dot{\theta} \end{bmatrix}$$

To evaluate the stability of the internal dynamics, set the desired output to zero and linearize the internal dynamics by linearizing about the original as:

$$\frac{d}{dt}\eta = \begin{bmatrix} 0 & 1 \\ \gamma^2 & 0 \end{bmatrix}\eta = A_\eta \eta$$

Where

$$\gamma^2 = \frac{\lambda Mg}{J}$$

And in order to find bounded solution for the internal dynamics, we can view internal dynamic as an additive perturbation on the linearized internal dynamics. The perturbation is as following:

$$s[\eta_n, y_d] - A\eta_n = \begin{bmatrix} 0 \\ p_n \end{bmatrix}$$

Like the internal dynamics itself, the linear equation also has an unstable equilibrium point. We explicitly find a bounded solution by first decomposing the linear ordinary differential equations into stable and unstable subsystems as:

$$\begin{aligned} \dot{z}_s &= -\gamma z_s - \frac{p_n}{2\gamma} \\ \dot{z}_u &= \gamma z_u + \frac{p_n}{2\gamma} \end{aligned}, \qquad \begin{bmatrix} z_s \\ z_u \end{bmatrix} = \frac{1}{2\gamma}\begin{bmatrix} \gamma & -1 \\ \gamma & 1 \end{bmatrix}\eta$$

And then flowing along the stable manifold forward in time and backward along the unstable manifold to obtain the only bounded solution for η and then inverse input
The whole iteration solving process is: $\eta_0 \to z \to \eta_1 \to z \to \eta_2 \to \cdots \to z \to \eta_n$

3.2 Preview-time approach

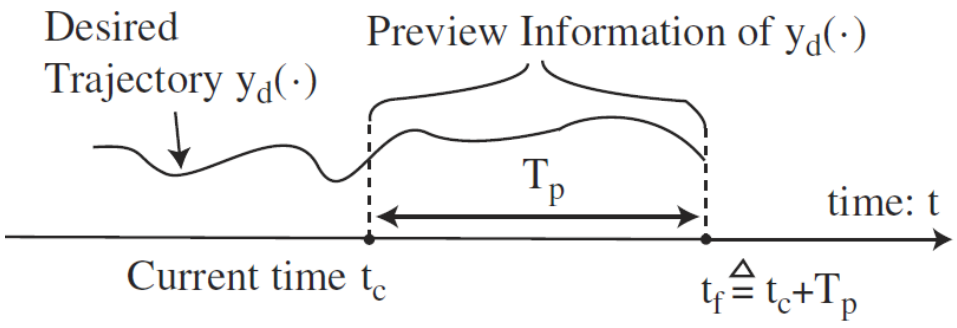

Figure 2. Preview time Method

The desired trajectory is known for a preview-time-window $t \in [t_c, t_c + t_p]$ as shown in above figure, and then the preview-based bounded solution to the nonlinear internal

dynamics is obtained as the limit of an iterative process. In particular, at each iteration step, we solve the following linear differential equation:

$$\dot{\eta}_{s,m} = -\gamma \eta_{s,m} - \frac{1}{2\gamma} p\left(\eta_{m-1}, \ddot{y}_d\right)$$

$$\dot{\eta}_{\mathrm{u},m} = \gamma \eta_{\mathrm{u},m} + \frac{1}{2\gamma} p\left(\eta_{m-1}, \ddot{y}_d\right)$$

By flowing the stable internal dynamics $\eta_{s,m}$ forward in time and the unstable internal dynamics $\eta_{\mathrm{u},m}$ backward in time, for time $t \in \left[t_c, t_c + t_p\right]$ as

$$\begin{aligned}
\eta_m(t) &= \begin{bmatrix} \eta_{s,m} \\ \eta_{\mathrm{u},m} \end{bmatrix} \\
&= \begin{bmatrix} e^{-\gamma(t-t_c)} \eta_s(t_c) - \frac{1}{2\gamma} \int_{t_c}^{t} e^{-\gamma(t-\tau)} p\left[\eta_{m-1}(\tau), \ddot{y}_d(\tau)\right] d\tau \\ -\frac{1}{2\gamma} \int_{t}^{t_c+t_p} e^{-\gamma(t-\tau)} p\left[\eta_{m-1}(\tau), \ddot{y}_d(\tau)\right] d\tau \end{bmatrix} \\
&= \phi\left[\eta_{m-1}(\bullet), \ddot{y}_d(\bullet)\right](t), \forall t \in \left[t_c, t_c + t_p\right]
\end{aligned}$$

Where the iteration is started by (initial step m=0)

$$\eta_0(t) = \begin{bmatrix} e^{-\gamma(t-\tau)} \eta_s(t_c) \\ 0 \end{bmatrix} \text{ for } t \in \left[t_c, t_c + t_p\right]$$

$$\eta_s(t_c) = -\frac{1}{2\gamma} \int_{-\infty}^{t_c} e^{-\gamma(t_c-\tau)} p\left[\eta(\tau), \ddot{y}_d(\tau)\right] d\tau$$

3.2.1 The number of the iteration and the amount of preview time

The dependence of the precision in the inversion process on both the number of iteration and the amount of preview time is quantified in the following theorem

Theorem 1. Let the internal dynamics be hyperbolic as in the VTOL case. Moreover, let the nonlinearity of the internal dynamics as well as the inverse input law be locally Lipschitz, i.e., there exits positive constants K_y, K_η, K_1, K_2 such that

$$\begin{aligned}
&\left\| u_{ff}\left(\eta(t), \ddot{y}(t)\right) - u_{ff}\left(\bar{\eta}(t), \ddot{\bar{y}}(t)\right) \right\|_\infty \\
&\le K_y \left\| \ddot{y}(t) - \ddot{\bar{y}}(t) \right\|_\infty + K_\eta \left\| \eta(t) - \bar{\eta}(t) \right\|_\infty \\
&\left\| p\left(\eta(t), \ddot{y}(t)\right) - p\left(\bar{\eta}(t), \ddot{\bar{y}}(t)\right) \right\|_\infty \\
&\le K_2 \left\| \ddot{y}(t) - \ddot{\bar{y}}(t) \right\|_\infty + K_1 \left\| \eta(t) - \bar{\eta}(t) \right\|_\infty
\end{aligned}$$

For all time t and for any bounded functions satisfying $\left\|\ddot{y}(\bullet)\right\|_\infty < r, \left\|\ddot{\bar{y}}(\bullet)\right\|_\infty < r, \left\|\eta(\bullet)\right\|_\infty < r, \left\|\bar{\eta}(\bullet)\right\|_\infty < r$. If the constants K1 and K2 satisfy

$$\left(K_1 + K_2\right)/2 < 1$$

Then the following results hold:

i) there exists a locally unique fixed point $\eta^*(\bullet)$ of the mapping $\zeta\left[\eta(\bullet), \ddot{y}_d(\bullet)\right](\bullet)$, such that

$$\eta^*(t) = \zeta\left[\eta(\bullet), \ddot{y}_d(\bullet)\right](t), \text{for } \forall t \in \left[t_c, t_f\right]$$

And this fixed point can be found by using the finite-preview based Picard like iteration process;

ii) furthermore, this fixed point is a bounded solution to the internal dynamics;

iii) at any given time instant, the error between the exact inverse input, and the preview-based stable-inverse input, obtained with a finite preview time and a finite number of iteration s, is bounded as

$$e_{ff,\mathrm{m}}(t_c) \triangleq \left\| u_{e,ff}(t_c) - u_{ff,m}(t_c) \right\|_\infty$$

$$\leq K_\eta \frac{K_2}{2-K_1}\left[\frac{2(K_1/2)^m}{2-K1} + \frac{e^{-\hat{\gamma}T_p}}{1-\delta_\gamma}\right]\left\|\ddot{y}_d(\bullet)\right\|_\infty$$

Where

$$\hat{\gamma} \in \left(0, (1-K_1/2)\gamma\right), \delta_\gamma = \frac{K_1\gamma}{2(\gamma-\hat{\gamma})}$$

And in simple case, there is another way to estimate the preview-time, i.e., use settling time which is calculated by the following equation:

$$t_{settling} \approx \frac{4}{s}$$

Where

S= the distance between unstable zeros and image axis

IV. Simulation

4.1 Desired Trajectory

The designed trajectory is a half circle. Propose of control is that VTOL can track this half circle as moving path and follow it from (0, 1) to (1, 1) like figure 3. The VTOL system is nonlinear and non-minimum phase, and two methods will be used to control VTOL to track this designed trajectory.

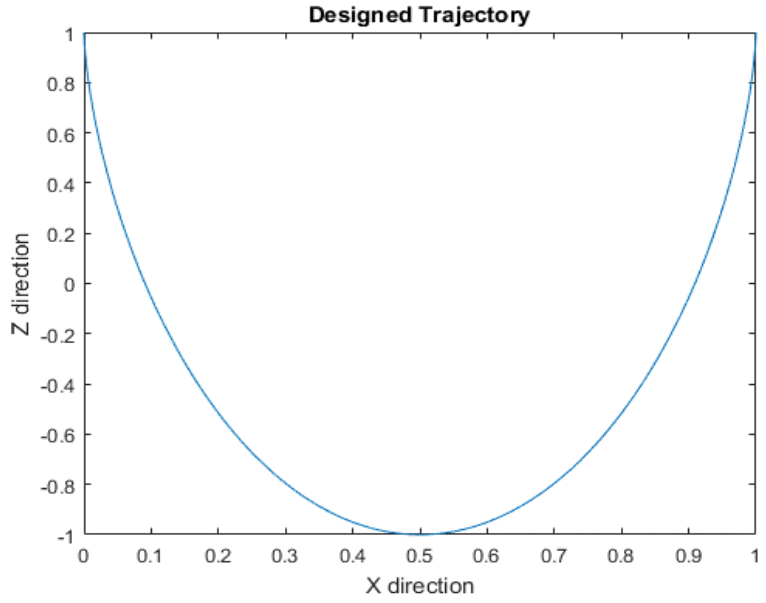

Figure.3. Designed Trajectory

4.2 Parameter Varied

Cross coupling term between rolling moment and lateral forces, ε, can be varied by different VTOL system. There are two different ε value, 0.5 and 0.05. Comparing with figure 4 and figure 5, smaller ε will has smaller output tracking error.

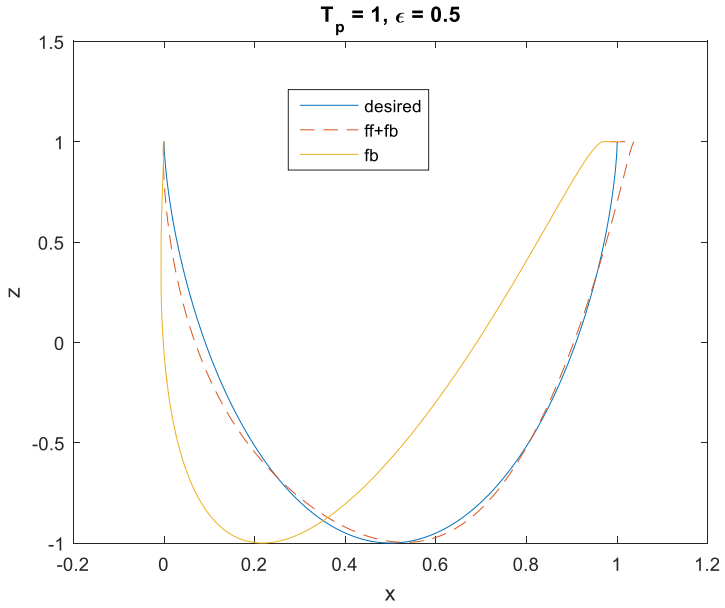

Figure.4. Actual Output VS Desired Trajectory ε=0.5

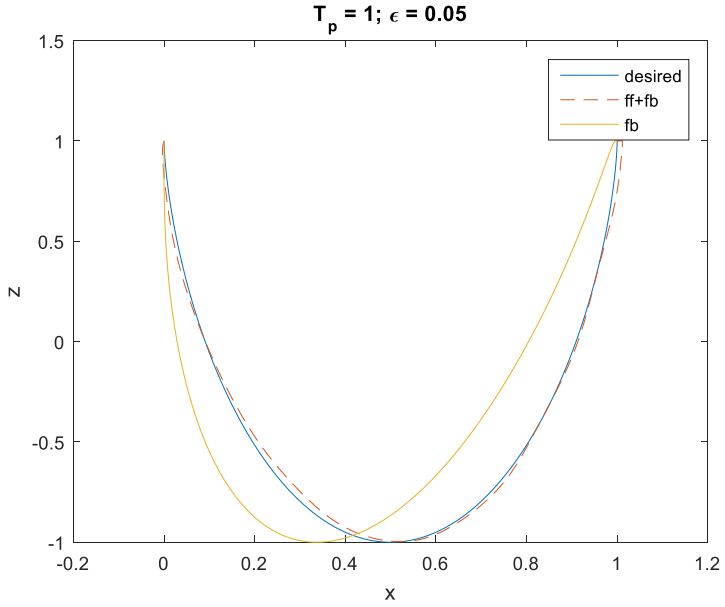

Figure.5. Actual Output VS desired trajectory ε=0.05

4.3 Feedforward Method discussion

These two methods are very similar, preview time method has the smaller Tp than another method. For the iteration method, we can think Tp is infinite, which means we don't need to move preview window to next step to simulate feedforward input. And for preview method, there is finite preview window width. So to control whole system based

on trajectory, we need to move preview window to simulate input for whole trajectory period. Because of limitation of sensor or prediction ability, preview time may not be able to infinite for real-time case and this control method is important for feedforward control application. There are several different Tp for preview time method, Tp=0.8s (figure 6),Tp=4s (figure 7) and Tp=8s (figure 8). On the plot x axis is location in x direction, and y axis is location in z direction. Blue curve is our designed trajectory which is figure 3. The golden curve is feedback alone output, which is LQR feedback method. And dashed curve is feedback and feedforward control output. From these three figures, when Tp increases, tracking will become better. When Tp=8, the output of feedforward and feedback control tracks desired trajectory very well.

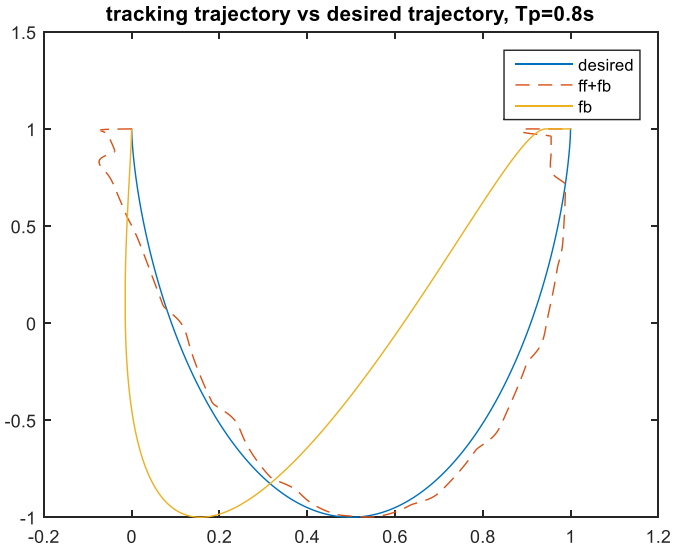

Figure 6. Actual Tracking VS desired trajectory Tp=0.8s

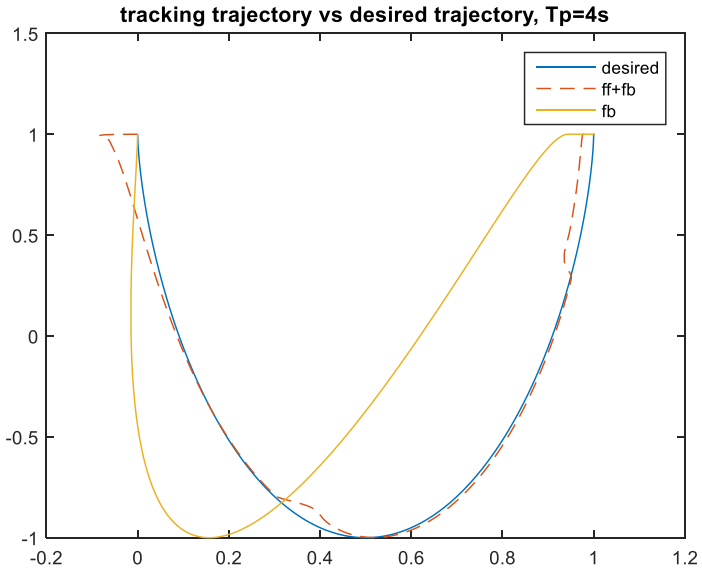

Figure 7. Actual Tracking VS desired trajectory Tp=4s

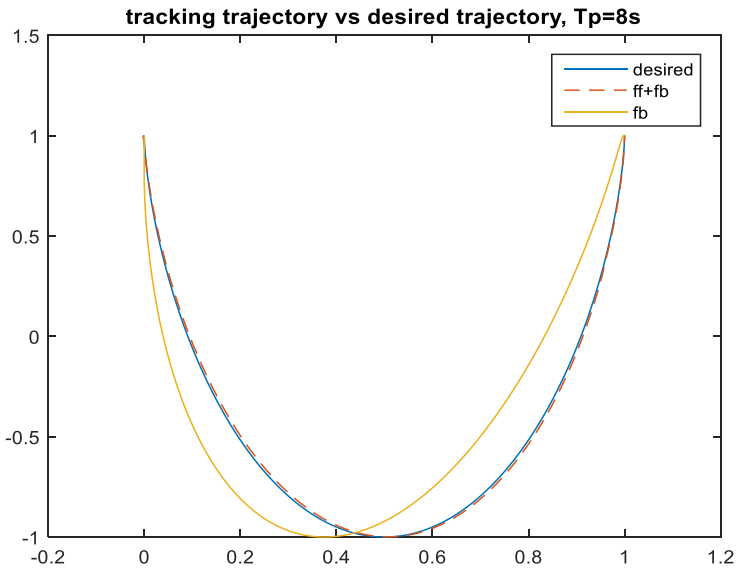

Figure 8. Actual Tracking VS desired trajectory Tp=8s

V. Summary

For final result, Tp of preview time method is 8s and m is 11. The feedback control is LQR with K matrix.

$$K = \begin{bmatrix} 0 & 0 & 316.2278 & 25.1487 & 0 & 0 \\ -316.2278 & -226.7874 & 0 & 0 & 797.7686 & 257.8210 \end{bmatrix}$$

And error plot shows in figure 9. The z direction tracking error is mirror that the largest tracking error is 0.0025. And x direction tracking error is slightly larger than z direction tracking error with 0.02 largest tracking error. Because error of two directions is very small, the actual feedforward and feedback control output tracks desired trajectory very well in figure 8.

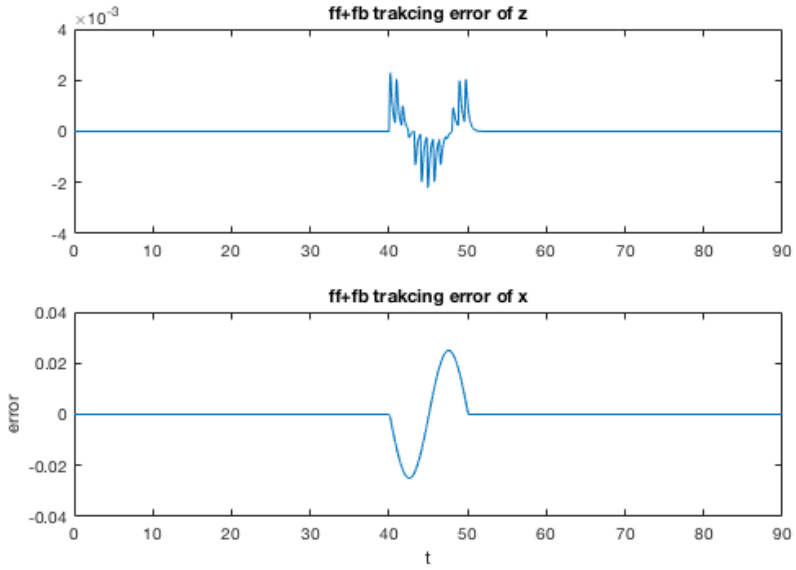

Figure 9. Feedforward+Feedback Control error

Thus practically, preview time is more realistic because we usually can't get the whole desired trajectory which means we can't use the infinite window method to track the desired trajectory.

Bibliography

[1] J. Hauser, S. Sastry, G. Meyer, "Nonlinear Control Design for Slightly Non-minimum Phase Systems: Application to V/STOL Aircraft," Automatica, Vol. 28, No. 4, pp. 665-679, 1992.

[2] P. Martin, S. Devasia, B. Paden, "A Different Look at Output Tracking: Control of a VTOL Aircraft," Automatica, Vol. 32, No. 1, pp. 101-107, 1996.